





Ambra1 modulates the tumor immune microenvironment and response to PD-1 blockade in melanoma

Alex Frias,¹ Luca Di Leo ,¹ Asier Antoranz,² Loulieta Nazeraï ,¹ Marco Carretta,³ Valérie Bodemeyer,¹ Chiara Pagliuca ,¹ Christina Dahl,⁴ Giuseppina Claps,⁵ Giulio Eugenio Mandelli,² Madhavi Dipak Andhari,² Maria Pires Pacheco,⁶ Thomas Sauter,⁶ Caroline Robert,⁵ Per Guldberg,^{4,7} Daniel Hargbøl Madsen,³ Francesco Cecconi,^{8,9} Francesca Maria Bosisio,² Daniela De Zio ,^{1,10}

To cite: Frias A, Di Leo L, Antoranz A, *et al.* Ambra1 modulates the tumor immune microenvironment and response to PD-1 blockade in melanoma. *Journal for ImmunoTherapy of Cancer* 2023;**11**:e006389. doi:10.1136/jitc-2022-006389

► Additional supplemental material is published online only. To view, please visit the journal online (<http://dx.doi.org/10.1136/jitc-2022-006389>).

Accepted 21 February 2023

ABSTRACT

Background Loss of Ambra1 (autophagy and beclin 1 regulator 1), a multifunctional scaffold protein, promotes the formation of nevi and contributes to several phases of melanoma development. The suppressive functions of Ambra1 in melanoma are mediated by negative regulation of cell proliferation and invasion; however, evidence suggests that loss of Ambra1 may also affect the melanoma microenvironment. Here, we investigate the possible impact of Ambra1 on antitumor immunity and response to immunotherapy.

Methods This study was performed using an Ambra1-depleted *Braf*^{N600E}/*Pten*^{-/-} genetically engineered mouse (GEM) model of melanoma, as well as GEM-derived allografts of *Braf*^{N600E}/*Pten*^{-/-} and *Braf*^{N600E}/*Pten*^{-/-}/*Cdkn2a*^{-/-} tumors with Ambra1 knockdown. The effects of Ambra1 loss on the tumor immune microenvironment (TIME) were analyzed using NanoString technology, multiplex immunohistochemistry, and flow cytometry. Transcriptome and CIBERSORT digital cytometry analyses of murine melanoma samples and human melanoma patients (The Cancer Genome Atlas) were applied to determine the immune cell populations in null or low-expressing AMBRA1 melanoma. The contribution of Ambra1 on T-cell migration was evaluated using a cytokine array and flow cytometry. Tumor growth kinetics and overall survival analysis in *Braf*^{N600E}/*Pten*^{-/-}/*Cdkn2a*^{-/-} mice with Ambra1 knockdown were evaluated prior to and after administration of a programmed cell death protein-1 (PD-1) inhibitor.

Results Loss of Ambra1 was associated with altered expression of a wide range of cytokines and chemokines as well as decreased infiltration of tumors by regulatory T cells, a subpopulation of T cells with potent immunosuppressive properties. These changes in TIME composition were associated with the autophagic function of Ambra1. In the *Braf*^{N600E}/*Pten*^{-/-}/*Cdkn2a*^{-/-} model inherently resistant to immune checkpoint blockade, knockdown of Ambra1 led to accelerated tumor growth and reduced overall survival, but at the same time conferred sensitivity to anti-PD-1 treatment.

Conclusions This study shows that loss of Ambra1 affects the TIME and the antitumor immune response in

WHAT IS ALREADY KNOWN ON THIS TOPIC

⇒ Autophagy and beclin 1 regulator 1 (Ambra1) is a scaffold protein that participates in several oncogenic processes, including autophagy, apoptosis, cell proliferation, and invasion. In preclinical mouse models of melanoma, we previously showed that *Ambra1* loss accelerates tumor growth and progression by stabilizing cyclin D1, activating focal adhesion kinase 1 signaling, and promoting the extracellular matrix remodeling and the epithelial-mesenchymal transition (EMT) process.

WHAT THIS STUDY ADDS

⇒ In this study, we show that Ambra1 deficiency affects the tumor immune microenvironment in melanoma by reshuffling the cytokine expression and decreasing regulatory T cells (Treg) tumor infiltration in an autophagy-dependent manner. Moreover, we show that anti-programmed cell death protein-1 immunotherapy reduces the growth of Ambra1-deficient tumors.

HOW THIS STUDY MIGHT AFFECT RESEARCH, PRACTICE, OR POLICY

⇒ This study highlights the complex role of Ambra1 in melanoma biology and emphasizes Treg as a promising target for immunotherapy efficacy.

melanoma, highlighting new functions of Ambra1 in the regulation of melanoma biology.

INTRODUCTION

Melanoma is an aggressive type of melanocyte-derived cancer, most often located in the skin and causing thousands of deaths worldwide every year. A common feature of melanoma is the constitutive activation of the MAPK and PI3K/AKT pathways, primarily through activating mutations of the BRAF kinase (*e.g.*, the *BRAF*^{V600E} in >90% of cases) and loss of the tumor-suppressing phosphatase PTEN,



© Author(s) (or their employer(s)) 2023. Re-use permitted under CC BY-NC. No commercial re-use. See rights and permissions. Published by BMJ.

For numbered affiliations see end of article.

Correspondence to

Professor Daniela De Zio; dzio@cancer.dk

respectively.^{1,2} Chemical inhibitors targeting components of the MAPK pathway, for example, BRAF and MEK, have shown limited clinical efficacy, when employed as either a single treatment or in combination with other therapies.³ However, treatment options for melanoma have rapidly expanded with the approval of various forms of immunotherapy. In particular, the use of antibody-based immunotherapy (immune-checkpoint blockade, ICB) has resulted in a dramatic survival improvement for patients with advanced melanoma.^{4,5} Two main classes of ICB antibodies are currently applied in the clinic: anti-CTLA-4 (cytotoxic T lymphocyte-associated antigen 4) and anti-PD-1/PD-L1 (programmed cell death protein 1/programmed cell death protein ligand 1).⁶ Their respective mechanism of action relies on reversing the inhibitory effect of CTLA-4 and PD-1/PD-L1 on T cells, hence inducing T-cell activation and expansion, ultimately supporting inflammation and immune cell infiltration of the tumor.⁶

Despite being beneficial for a minority of melanoma patients experiencing durable responses, most show minimal or no response to ICB.⁷ Several lines of evidence suggest that one cause of interpatient differences in ICB responsiveness may be differences in the composition of the tumor immune microenvironment (TIME).⁷⁻⁹ Flow cytometry and imaging technologies have indeed revealed pronounced TIME interpatient heterogeneity, both in terms of tumor cell-intrinsic expression of signaling molecules (e.g., chemokines and cytokines), which may be controlled by the profile of oncogenic drivers in individual tumors, and cellular components.^{7,9} Infiltration of some immune cell types, most importantly cytotoxic T cells, clearly associates with positive ICB response.⁸ On the other hand, tumor-resident myeloid-derived suppressor cells and regulatory T cells (Treg) block the antitumor immune response thereby promoting tumor growth and metastasis.^{4,8}

Recently, we have shown that *Ambra1* (autophagy and beclin 1 regulator 1) plays a central role in nevi formation and melanoma, as its absence accelerates tumor growth and metastasis.¹⁰ *Ambra1* is a scaffold protein regulating several biological processes, including autophagy, cell death and proliferation and invasion.¹¹⁻¹⁷ Loss of *Ambra1* increases cell cycle progression by regulating c-Myc and cyclin D1 stability and increases melanoma aggressiveness by enhancing cell motility and invasion. In addition, it promotes extracellular matrix remodeling and triggers focal adhesion kinase 1 (FAK1) signaling, the inhibition of which reduces cell invasion and melanoma growth.¹⁰ In this study, we analyze the complex landscape of the TIME of *Ambra1*-deficient melanoma by studying its composition and signaling. We also investigate whether the *Ambra1*-dependent immune signature affects the response to PD-1 inhibitor therapy in a preclinical mouse model of melanoma.

MATERIALS AND METHODS

Mice

The transgenic mice used for the study were C57BL/6N female and male. Breeding pairs were set to generate

mice bearing the *Tyr:CreER^{T2/+};Braf^{V600E/+};Pten^{-/-}* background with different *Ambra1* flox copy number, herein referred to as *BPA^{+/+}* (proficient for *Ambra1*, *Ambra1^{+/+}*) or *BPA^{-/-}* (KO for *Ambra1*, *Ambra1^{-/-}*).¹⁰ Animals were maintained and treated as previously reported.¹⁰ Regarding the syngeneic models, 8–10 weeks old C57BL/6N male mice were purchased from Taconic. Animals were allowed to acclimate in the facility before being subcutaneously injected in the right flank with either 2–5×10⁶ BPA-derived cells (*Ambra1* proficient, BPA-derived melanoma cells (Bdmc)^{+/+}, or *Ambra1* KO, Bdmc^{-/-}) or 1–1.5×10⁵ engineered shCT/sh*Ambra1* YUMM1.7 cells (see the Cell lines section). Mice were monitored as previously described.¹⁰ All mice were housed at the Danish Cancer Society Research Center and the experiments were performed in compliance with institutional guidelines and approved by the Danish animal experiments inspectorate (Dyreforsøgstilsynet, 2020-15-0201-00578).

Primary melanoma cells isolation

Tumors were excised from *BPA^{+/+}* and *BPA^{-/-}* mice and the skin was carefully removed. Tumors were fragmented and digested as previously described.¹⁰ Cells were kept in culture in RPMI 1640 supplemented with 100 U/mL penicillin/streptomycin (P/S) and 2–20% fetal bovine serum (FBS). Cells derived from *BPA^{+/+}* and *BPA^{-/-}* mice are referred to as Bdmc^{+/+} and Bdmc^{-/-} cells, respectively. To inhibit autophagy, Bdmc^{+/+} cells were treated for 48 hours with ddH₂O-dissolved chloroquine (CQ, Sigma-Aldrich; cat# C6628) at a final concentration of 5 μM.

Anti-PD-1/isotype control

When tumors reached measurable size (ca. 30 mm³), mice were treated with 10 mg/kg of anti-PD-1 (InVivoMAb anti-mouse PD-1 (CD279), Bio X Cell) by intraperitoneal injection. Control animals were treated with 10 mg/kg of IgG2a isotype (InVivoMAb rat IgG2a isotype control, Bio X Cell). After the first injection, mice received injections every third day for a total of approximately 2–4 weeks, depending on the duration of the study.

MILAN multiplex staining and image analysis

Tumor samples were collected and fixed overnight in paraformaldehyde (PFA) 4% at 4°C, followed by three washes in phosphate buffered saline (PBS), and stored in 70% ethanol (ETOH) until embedded in paraffin. Formalin-fixed paraffin-embedded sections of 4 μm were cut and multiplexed immunofluorescent staining was performed according to the MILAN protocol.¹⁸ A brief description of this method, as well as a complete list of antibodies, is reported in online supplemental materials and methods.

Flow cytometry

Pieces of tumors were collected and digested overnight in digestion buffer (2.1 mg/mL collagenase type I (Worthington), 75 μg/mL DNAase I (Worthington), 5 mM CaCl₂ and 1% P/S in RPMI). The following day, samples were incubated for 15 min at 37°C and filtered through

a 70 µm nylon cell strainer and erythrocytes lysed using the red blood cells (RBC) lysing buffer (Sigma) for 1–2 min. Splenocytes (isolated from spleens of female mice) were instead generated by forcing freshly isolated spleens through 70 µm cell strainers and erythrocytes lysed using RBC lysing buffer for 1 min. Following centrifugation, cells (tumor/splenocytes) were washed and eventually resuspended in PBS. Single-cell suspensions from tumors/spleens were stained for 30 min (4°C in the dark) for relevant cell-surface markers in Fluorescence-activated cell sorter (FACS) staining buffer (PBS with 7% FBS). Next, cells were washed, resuspended in PBS and stored at 4°C until flow cytometric analyses were performed on the same day. All samples were acquired on Cytex Aurora equipped with four lasers (Cytex Biosciences) or by FACSCanto II cell Analyzer BD and analyzed with FlowJo V.10.6.1 or V.10.8 software. Viable cells were determined as a fraction of single cells negative for staining with Zombie Aqua Fixable Viability Dye. The immune cell populations were analyzed in three different panels: Panel 1 (general panel), Panel 2 (myeloid panel) and Panel 3 (lymphoid panel), which are described in online supplemental materials and methods. All cells were gated on singlets, living cells and the corresponding gating strategy for each cell population.

Splenocyte extraction and T-cell migration

Spleens were extracted from 10- to 12-week-old female C57BL/6N mice (Taconic). Single-cell suspensions of splenocytes were generated as described above. To enrich T cells population and induce their proliferation, isolated splenocytes were incubated overnight in RPMI 1640 (Life Technologies) supplemented with 10% FBS (Life Technologies), 1% P/S (Thermo Fisher Scientific), 50 µM 2-ME (Sigma-Aldrich), 0.1 mM non-essential amino acids (Thermo Fisher Scientific), 1 mM sodium pyruvate (Thermo Fisher Scientific)—referred to as ‘T cell medium’—and 3 µg/mL ConA (Sigma-Aldrich). The migration of T cells towards the conditioned medium from BPA melanoma cells was measured using overnight-rested primary murine T cell isolated as described. Conditioned media were harvested from Bdmc^{+/+} and Bdmc^{-/-} grown until confluence. A detailed description of the protocol is reported in online supplemental materials and methods.

Cell lines

YUMM1.7 cells were purchased from American Type Culture Collection (ATCC) (Manassas, Virginia, USA) and cultured in DMEM (Thermo Fisher Scientific, Massachusetts, USA) supplemented with 2 mM GlutaMAX (Thermo Fisher Scientific, Massachusetts, USA), 7% FBS (Thermo Fisher Scientific, Massachusetts, USA) and 100 U/mL P/S (Thermo Fisher Scientific, Massachusetts, USA) at 37°C and 5% CO₂. Lentiviral expression in YUMM1.7 cell line was performed to stably knock down Ambra1 using shRNAs (#1: TRCN189905 and #3: TRCN189704 (Sigma)) cloned in a pLKO.1-puro vector (Mission; Sigma). Cells

grown to 60% confluency were infected overnight in the presence of polybrene at a final concentration of 8 µg/mL. Next day, the medium was removed and replaced by fresh medium to let cells recover. After 48 hours, infected cells were selected with 1.5 µg/mL puromycin. Cells were expanded under selection (between 6 and 21 days after infection) and puromycin was removed at least 48 hours before any experiment.

Human melanoma cell lines MeWo (ATCC HTB-65) and SK-Mel-5 (ATCC HTB-70) were purchased from ATCC and cultivated in minimum essential media (MEM) (Thermo Fisher Scientific, Massachusetts, USA) supplemented with 2 mM GlutaMAX, 10% FBS and 100 U/mL P/S. Cells were cultured in an atmosphere of 5% CO₂ in air at 37°C. All the cell lines were routinely tested for *Mycoplasma* contamination (Eurofins Genomics, Germany).

Transfection methods

Transfections were carried out using the Lipofectamine 2000 Transfection Reagent (Thermo Fisher Scientific, Massachusetts, USA; cat# 11668–019), according to the manufacturer’s instructions. Transfections with siRNAs were performed as previously reported,¹⁰ with the following custom-designed siRNAs: siAMBRA1: 5'-GGC CUA UGG UAC UAA CAA A -3'; siAMBRA1 #2: 5'-GGA CAA CUU ACA AGG ACC -3'. Silencing was carried out for 48 hours. Generation and transfection of AMBRA1 mutants were carried out as described in a study by Tiberti *et al.*¹⁹ After 24 hours from transfection of cells with siAMBRA1 #2, re-expression of the mutants was performed for a total of 24 hours; a myc-β-Gal plasmid cloned in the pcDNA3.1 Mammalian Expression Vector (Thermo Fisher Scientific, Massachusetts, USA; cat# V79020) was used as negative control.

Protein expression analysis

Total protein lysates from cell pellets and murine tissues were obtained as previously described.¹⁰ Primary antibodies used are listed in online supplemental materials and methods. Densitometry analyses were performed using ImageJ (V.1.52.q). The LC3 ratio was calculated as the ratio of the densitometry values of the lipidated (LC3-II) and the non-lipidated (LC3-I) form of LC3. Densitometries of pFAK and pSRC were calculated as the ratio of the densitometry values of the phosphorylated form of the protein (pFAK1-Y397 and pSRC-Y416, respectively) and its total (FAK1 and SRC, respectively). Densitometry values (and ratios) were normalized against their respective loading control and expressed as fold change relative to the control sample.

Nuclei isolation

Cells were transfected as described above for 48 hours and nuclear fractions were isolated as described in a study by Di Leo *et al.*²⁰ Nuclear fractions were then disrupted in radioimmunoprecipitation assay (RIPA) buffer and SDS-PAGE electrophoresis was performed. Based on protein quantification, total extract (TE), post-nuclear

(cytosolic) (CE) and nuclear (NE) fractions were loaded onto the gel using a 4:3:1 ratio ($\mu\text{g}:\mu\text{g}:\mu\text{g}$), respectively. For determination of the purity of each fraction, primary antibodies raised against lactate dehydrogenase (LDH) (specific for the CE; Santa Cruz Biotechnology, cat# sc-33781) and lamin A/C (specific for the NE; Santa Cruz Biotechnology, cat# sc-6215) were employed. Densitometry analyses were performed using ImageJ (V.1.52.q). The nuclear fraction of FAK1 was calculated as the ratio between the normalized densitometry values of FAK1 on lamin A/C in the NE and in the TE. Similarly, the CE fraction of FAK1 was calculated as the ratio between the normalized densitometry values of FAK1 on LDH in the CE and in the TE.

Cytokine array

The profiling of different cytokines and chemokines was performed using the Proteome Profiler Mouse/Human Cytokine Array Kit (R&D systems, cat# ARY006 and cat# ARY005B, respectively) according to the manufacturer's instructions. Supernatants were harvested from an equal number of cells 72 hours after seeding, treating, or transfecting cells, depending on the experimental conditions. Images were taken using a ChemiDoc MP System (Bio-Rad Laboratories, California, USA; cat# 1708–280) provided with the Image Lab V.6.0.1 Software (Bio-Rad Laboratories, California, USA). The signal intensities of the spots were quantified using ImageJ V.1.52.q (University of Wisconsin, Wisconsin, USA). Gene set enrichment analysis was performed using hypergeometric tests.

RNA isolation

For real-time quantitative PCR (RT-qPCR) analyses, total RNA was isolated directly from culture cells using the NucleoSpin RNA Columns (Macherey-Nagel, DE; cat# 740955) according to the instructions of the manufacturer. For NanoString profiling, RNA from tissues (disrupted with Qiagen TissueLyser II) were isolated using the RNeasy Plus Mini Kit (Qiagen, DE; cat# 74134), following manufacturer's instructions. When RNA from tissues could not be isolated at the moment, tumor pieces were preserved in RNAlater Stabilization Solution (Thermo Fisher Scientific, Massachusetts, USA; cat# AM7020), according to the instructions.

Reverse transcription and quantitative RT-PCR

Reverse transcription was performed for 1 hour at 37°C with 500 ng of total RNA with the M-MLV Reverse Transcriptase (Promega, Wisconsin, USA; cat# M1705) and diluted 3X before any RT-qPCR analysis. Messenger RNA (mRNA) expression levels from mouse samples were measured using the PowerUp SYBR Green Master Mix (Thermo Fisher Scientific, Massachusetts, USA; cat# A25742), according to the instructions, on a ViiA 7 Real-Time PCR System (Applied Biosystems, California, USA). Fold changes in mRNA levels relative to the control were calculated after normalizing to the housekeeping gene *L34*. Expression of *IL-1 α* from human

samples was assessed using a LigthCycler V.2.0 with the FastStart DNA Master^{PLUS} SYBR Green I kit (Roche) and normalized to the housekeeping gene *RPLP0*. All reactions were run as triplicates. The specific primer pairs were custom designed and tested with Primer-BLAST (NCBI; RRID:SCR_003095). Primers used were obtained from TAG Copenhagen A/S (Copenhagen, DK) and are as follows: Ccl22 (mouse) FW 5'- TCTTGCTGTGGCAATTCAGA -3', RV 5'- GAGGGTGACGGATG-TAGTCC -3'; L34 (mouse) FW 5'- GGTGCTCAGAGG CACTCAGGATG -3', RV 5'- GTGCTTTCCCAACCTT CTTGGTGT -3'; IL-1 α (human) FW 5'- ACGGCTGA GTTTCAGTGAGACC -3', RV 5'- CACTCTGGTAGG TGTAAGGTG -3'; RPLP0 (human) FW 5'- ACTAAAT CTCCAGGGGCACC -3', RV 5'- ATGACCAGCCCAAAG-GAGAA -3'.

NanoString data and bioinformatic analysis

NanoString data were processed at BioXpedia A/S. Two different NanoString Panels were used: PanCancer Immune (769 genes) and Immunology (560 genes) panel. Data reported in the heatmap were based on differentially expressed genes (comparing BPA^{-/-} to BPA^{+/+}) with $\text{padj} < 0.05$. NanoString data are illustrated in the online supplemental tables 1 and 2.

The NanoString software nSolver was used for quality control (QC) and normalization of the data. For gene expression data, filtering of samples using QC criteria was performed according to the manufacturer's recommendations. Raw counts of samples passing QC were normalized by scaling the sample values to the geometric mean of the following selected reference genes (used as internal controls): *Abcf1*, *Alas1*, *Edc3*, *Eef1g*, *Eif2b4*, *G6pdx*, *Gusb*, *Hdac3*, *Hprt*, *Nubp1*, *Oaz1*, *Polr1b*, *Polr2a*, *Ppia*, *Rpl19*, *Sap130*, *Sdha*, *Sf3a3*, *Tbp*, *Tubb5*. The reference genes (20 for the PanCancer Immune and 14 for the Immunology panel) were selected using the geNorm algorithm.²¹ Data were log₂-transformed and further analyzed. Differential expression analysis (DEA) was made in R V.3.5.1 (2018-07-02). Student's t-test was applied to compare normalized expression values between groups. For all the t-tests, normal distribution among the two tested groups was first checked using the Shapiro-Wilk test. If one of the groups was not normally distributed, a Wilcoxon rank-sum test was conducted instead. Furthermore, the fold change was calculated on a linear scale as the geometric mean of the first group divided with the geometric mean of the second group. The p values were corrected for multiple testing using the Benjamini-Hochberg method. Pathway analysis was performed with the online tool Enrichr (Icahn School of Medicine at Mount Sinai, New York, USA) (GO_Process) and gene set enrichment (GSE PIANO).²² For the estimation of cell type percentages in bulk samples via digital cytometry we used CIBERSORT²³ with the standard LM22 signature matrix and B-mode for batch effect correction.

RNA sequencing and analysis

The RNA sequencing (RNA-seq) data from BPA^{+/+} and BPA^{-/-} samples were previously generated¹⁰ and are publicly available under the Gene Expression Omnibus (GEO) accession number GSE151134. DEA was performed with R Bioconductor package DESeq2 and pathway analysis was performed with the online tool Enrichr (Icahn School of Medicine at Mount Sinai, New York, USA). A detailed description of the parameters used for each analysis and the processing of the RNA-seq has already been published.¹⁰

The RNA-seq data were also uploaded to Ingenuity Pathway Analysis (IPA, <https://www.nihlibrary.nih.gov/resources/tools/ingenuity-pathways-analysis-ipa>) and the core analysis was performed with default settings with a Benjamini-Hochberg corrected p value cut-off of 0.05 for target enrichment. The obtained list of active upstream regulators was filtered for differential expression of the regulators ($|\text{abs}(\log_2 \text{fold change})| \geq 1$; adjusted p value ≤ 0.05) and overlapped with a list of transcription factors (TFs) obtained from AnimalTFDB.²⁴

In silico analyses using publicly available data sets

RNAseq data for skin cutaneous melanoma (SKCM) samples were downloaded from The Cancer Genome Atlas (TCGA) and preprocessed with the TCGAbiolinks R package V.2.18.0. For the estimation of cell type percentages in bulk samples via digital cytometry we used CIBERSORT²³ with the standard LM22 signature matrix and B-mode for batch effect correction. The cut-off selection in Treg and AMBRA1 expression was performed by evaluating all possible cut-offs. For each cut-off we obtained a p value (Wilcoxon test). The negative log₁₀ of the p value was smoothed by applying a running average and therefore reducing potential overfitting. In the running average, the maximum of the negative log₁₀ p value was selected and the corresponding value was used as cut-off. AMBRA1 expression levels were associated with response to anti-PD-1 immunotherapy in a cohort of patients with melanoma including RNA-seq samples from responders and non-responders to anti-PD-1 before and during the treatment.²⁵ Raw counts were downloaded from the GEO (GSE91061). Patient-derived metadata was downloaded from the authors' publication. Only patients with extreme response profiles (complete response (CR) and progressive disease (PD)) were used for the analysis. AMBRA1 expression was compared between both groups using Wilcoxon's test.

Statistical evaluation

GraphPad Prism Software (V.9) was used for plotting the graphs and performing the statistical analysis. For comparison of more than two-groups, a Tukey's multiple comparisons test (ordinary two-way analysis of variance (ANOVA) test) and unpaired t-test with Bonferroni-Dunn correction for multiple comparisons were performed. Pairwise comparisons were carried out using a non-parametric Mann-Whitney U test. For comparison of tumor growth

kinetics, two-way ANOVA with Bonferroni's multiple comparison test was performed. Data are presented as means \pm SD or \pm SEM (see figure legends for details) and significance was designated as follows: * $p \leq 0.05$; ** $p \leq 0.01$; *** $p \leq 0.001$; **** $p \leq 0.0001$; ns, not significant.

RESULTS

Loss of Ambra1 promotes downregulation of cytokine signaling in Braf/Pten-driven melanoma

To investigate the effect of Ambra1 deficiency on immune signaling in melanoma, we employed the NanoString technology. First, we characterized the immune-related transcriptome in Ambra1-deficient (BPA^{-/-}) and Ambra1-proficient (BPA^{+/+}) Braf/Pten-driven melanomas¹⁰ using the Immunology and PanCancer Immune Panels. In both panels, DEA showed a consistent profile of gene expression within groups with the same genetic background and a clear separation between BPA^{-/-} and BPA^{+/+} tumors (figure 1A,B and online supplemental figure 1A–C). Gene Ontology and GSE (PIANO) analyses of differentially expressed genes revealed several downregulated processes in Ambra1-deficient melanomas, including the cytokine-mediated signaling pathways and the inflammatory response, along with upregulated processes (e.g., transforming growth factor- β and integrin/focal adhesion signaling pathways), in line with our previous findings¹⁰ (figure 1C,D and online supplemental figure 1D,E). RNA-seq analyses from our previous study¹⁰ also showed the cytokine receptor activity among the most downregulated processes ($\text{padj} < 0.05$, $\text{FC} > 2$) in Ambra1-deficient tumors (online supplemental figure 1F). Accordingly, both NanoString and RNA-seq analyses pinpointed reduced expression of several cytokines and chemokines in BPA^{-/-} tumors (figure 1E).

Overall, these results suggest a decrease of cytokine/inflammatory signaling in Ambra1-deficient melanoma.

Decreased infiltration of Treg in Ambra1-deficient melanoma

Prompted by the differences in cytokine and chemokine expression, we characterized the immune cell populations in the TIME of BPA^{-/-} and BPA^{+/+} tumors. Preliminary immunofluorescence analysis of BPA^{-/-} and BPA^{+/+} tumors at the same endpoint (42 days after tumor induction) showed a slight increase in hematopoietic cells (CD45⁺) in Ambra1-deficient tumors (figure 2A). Flow cytometry analysis of tumors grown to the maximally tolerated size revealed instead a comparable number of CD45⁺ cells (with a trend to increase in BPA^{-/-}), endothelial cells (CD31⁺) and fibroblasts (FAP⁺) between the two groups (figure 2B and C). The CD45⁺ cells were further analyzed to discriminate among macrophages (F4/80⁺), dendritic cells (CD11c⁺) and myeloid cells (CD11b⁺), and to evaluate the lymphoid subset (CD3⁺ T-cells, NK1.1⁺ NK-cells and CD19⁺ B-cells). Flow cytometry analysis of both myeloid and lymphoid panels (figure 2D–G) indicated a significant decrease only for CD4⁺/CD25⁺ Treg in BPA^{-/-} melanomas (3.9% vs 32.1%) (figure 2F and G), with

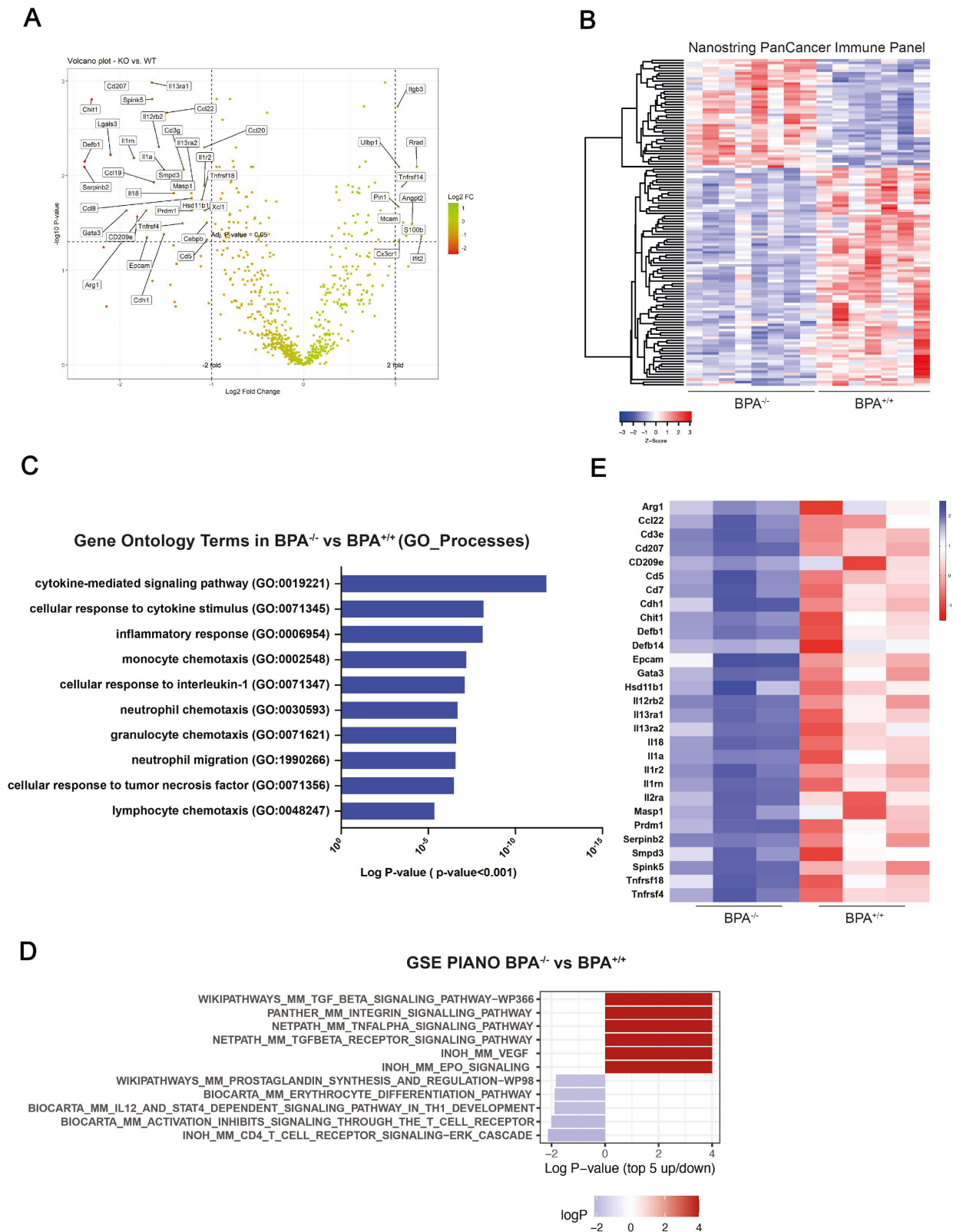


Figure 1 Characterization of immune signature in *Ambra1*-deficient melanoma. (A) Volcano plot and (B) heat map of differentially expressed genes (DEG) from NanoString PanCancer Immune Panel (769 genes) of BPA^{-/-} (n=8) versus BPA^{+/+} (n=7) tumors (padj<0.05). A total of 126 (85 down and 42 up) DEG were found in the PanCancer Immune Panel. (C–D) GO processes (downregulated, p<0.001) and GSE PIANO (top five upregulated/downregulated) in BPA^{-/-} (n=8) versus BPA^{+/+} (n=7) tumors analyzed with PanCancer Immune panel (FC>2). (E) DEG from NanoString PanCancer Immune and Immunology panels merged with DEG from RNA sequencing (BPA^{-/-} vs BPA^{+/+}), pdj<0.05, FC>2. *Ambra1*, autophagy and beclin 1 regulator 1; GO, Gene Ontology; GSE, gene set enrichment.

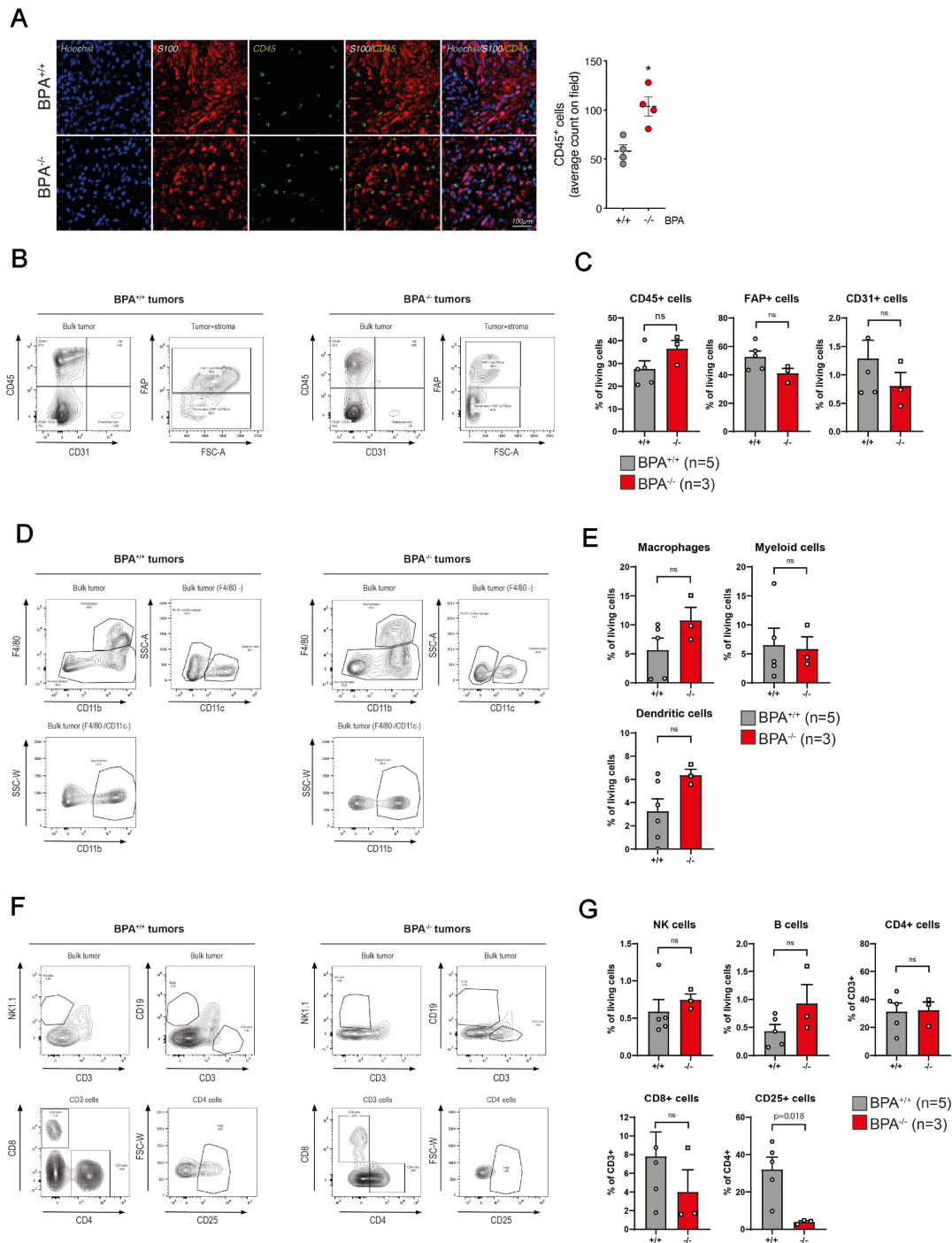


Figure 2 Analysis of immune cell populations in Ambra1-deficient melanoma. (A) Immune cells were assessed by CD45 immunostaining (green) in formalin-fixed paraffin-embedded tumor sections of BPA^{+/+} (n=4) and BPA^{-/-} (n=4) mice. Nuclei were counterstained with Hoechst (blue) and melanoma cells visualized with the melanoma marker S100 (red). Images are representative of each group. In the graph, the CD45 signal was quantified. Each data point represents one mouse and corresponds to the average ratio±SEM of CD45⁺ cells on the nuclei count for each mouse (at least three fields were analyzed for each mouse) (*p<0.05, BPA^{-/-} vs BPA^{+/+}). (B–G) Tumors from BPA^{+/+} (n=5) and BPA^{-/-} (n=3) groups were collected and processed for flow cytometric analysis. Viable cells were determined as a fraction of single cells negative for staining with Zombie Aqua Fixable Viability Dye. Quantification is reported as a percentage of indicated cell type among live cells or the parental gate. Representative flow plots on the gating strategy of (B) immune/tumors, (D) myeloid and (F) lymphoid cells in BPA^{+/+} and BPA^{-/-} groups. (C) % of CD45⁺, FAP⁺ (defined as CD45⁺FAP⁺), CD131⁺ (defined as CD45⁺CD131⁺) cells. (E) % of macrophages (defined as F4/F80⁺CD11b⁺), myeloid (defined as F4/F80⁻CD11c⁻CD11b⁺) and dendritic cells (defined as F4/F80⁻CD11c⁺). (G) % of NK cells (defined as CD3⁺NK1.1⁺) and B cells (defined as CD3⁺CD19⁺) out of the live cell population; % of CD4⁺ (defined as CD3⁺CD4⁺), CD8⁺ (defined as CD3⁺CD8⁺) and CD25⁺ (defined as CD3⁺CD4⁺CD25⁺) cells out of the parental gate. Each dot represents one mouse and corresponds to the mean±SEM (ns, not significant). Data were analyzed by unpaired t-test (BPA^{-/-} vs BPA^{+/+}). Ambra1, autophagy and beclin 1 regulator 1; NK, natural killer.

no evident changes in spleens of matched mice (online supplemental figure 2A,B). A significant reduction in CD4⁺/CD25⁺ Treg (5.8% vs 39.1%) was also observed in tumors from a C57BL/6 immunocompetent syngeneic mouse model of primary Bdmc (sBPA^{+/+} and sBPA^{-/-}; Ambra1-proficient and Ambra1-deficient, respectively)¹⁰ (online supplemental figure 3).

We next sought to visually map the relative spatial distribution of immune cell populations in sBPA^{-/-} and sBPA^{+/+} tumors by multiplexed-immunohistochemistry technology.^{18,26} In line with the flow cytometry results (figure 2F and G), FOXP3⁺CD4⁺ Treg were less abundant in sBPA^{-/-} tumors (figure 3A,B and online supplemental figure 4A), however not statistically significant. We next

performed IPA core analysis on murine RNA-seq data¹⁰ to identify putative TFs with altered activity in BPA^{-/-} tumors. Ten differentially expressed TFs with significant changes in their downstream targets were identified, among which the Treg marker *Foxp3*, with an enrichment corrected p value of 0.005 (figure 3C). This analysis suggests activity changes of the *Foxp3* TF in Ambra1-deficient tumors, along with its reduced expression.

To increase the human relevance of these findings, melanoma transcriptomic data from TCGA-SKCM data set (n=473) were analyzed via CIBERSORT digital cytometry to predict the relative content of Treg and to correlate their abundance to *AMBRA1* expression levels. When splitting the TCGA-SKCM samples in Treg-high and

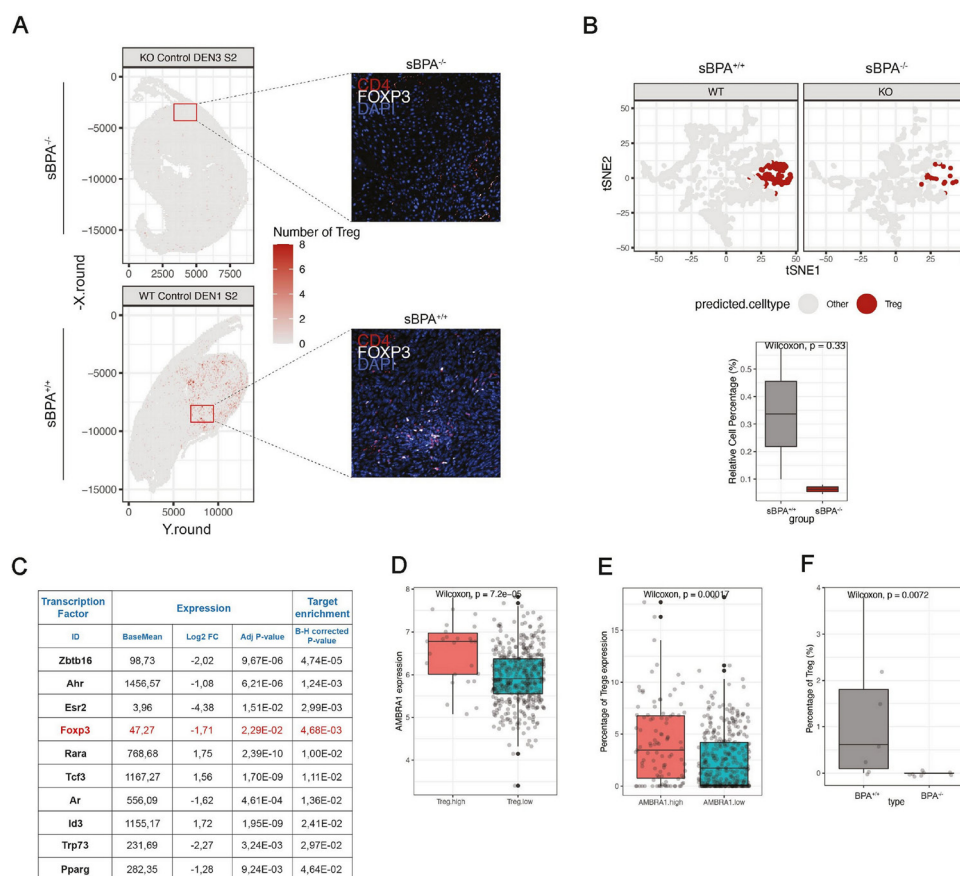


Figure 3 Analysis of Treg in Ambra1-deficient melanoma. (A–B) Tumors from syngeneic sBPA^{+/+} (WT, n=2) and sBPA^{-/-} (KO, n=2) mice were collected and processed for multiplex immunohistochemistry. (A) Illustrative representation of the number of Treg in each analyzed sample. Tissue samples were cut into squares of 66 μm² and the number of Treg was counted inside each square. (B) Five hundred cells were randomly selected from each identified cell type and dimensionally reduced using a t-SNE. The cells were projected in the t-SNE space by separating sBPA^{-/-} from sBPA^{+/+} samples. The % of Treg in each group is shown in the bar plot below. (C) IPA-based prediction of active upstream regulators, predicted from the RNA sequencing data with the IPA core analysis and filtered for differentially expressed transcription factors (see online supplemental material & methods). Putatively active TFs are listed showing their expression baseMean, log2 fold change (sBPA^{-/-} vs sBPA^{+/+}) and adjusted p value, as well as with the corrected p value for target enrichment as obtained from the IPA core analysis. (D) Boxplots representing *AMBRA1* expression for samples with high/low levels of Treg or (E) Treg percentages for samples with high/low expression of *AMBRA1* in the The Cancer Genome Atlas-skin cutaneous melanoma data set. (F) Boxplot representing the percentage of Treg in BPA^{-/-} and sBPA^{+/+} tumors estimated with CIBERSORT in the samples measured with the NanoString Immunology panel. Ambra1, autophagy and beclin 1 regulator 1; IPA, Ingenuity Pathway Analysis; KO, knockout; TFs, transcription factors; Treg, regulatory T cells; t-SNE, t-distributed stochastic neighbor embedding; WT, wild type.

Treg-low (online supplemental figure 4B, see methods), we found a positive correlation with *AMBRA1* expression levels (figure 3D). Similarly, when TCGA-SKCM samples were ranked in *AMBRA1*-high and *AMBRA1*-low (online supplemental figure 4C, see methods), a positive correlation with Treg abundance was found (figure 3E). Moreover, NanoString signature-based CIBERSORT deconvolution of *BPA*^{+/+} and *BPA*^{-/-} samples predicted reduced content of Treg cells ($p < 0.01$) in *BPA*^{-/-} tumors (figure 3F and online supplemental figure 4D).

Overall, these data indicate that *Ambra1* deficiency impairs the infiltration of Treg in *Braf*/*Pten*-driven melanoma.

Infiltration of Treg is determined by the status of *Ambra1* in melanoma cells

To unravel direct implications of melanoma cells in Treg infiltration of the TIME, conditioned media of *Ambra1*-deficient (*Bdmc*^{-/-}) and *Ambra1*-proficient (*Bdmc*^{+/+}) primary murine melanoma cells (online supplemental figure 5A) were profiled for cytokine secretion. *Ambra1* deficiency is associated with lower secretion of several cytokines, chemokines and interleukins (ILs) (figure 4A and B). GSE analysis of these results showed cytokines and inflammatory response as the most significant downregulated pathways upon absence of *Ambra1* (figure 4C), in line with the transcriptomic data in figure 1 and online supplemental figure 1. Next, a T-cell migration assay with T cell-enriched murine splenocytes incubated with conditioned media from primary melanoma cells was performed to assess the relation between cytokine composition of *Bdmc*^{-/-} cells and tumor infiltration by T cells. As shown in figure 4D, CD4⁺ (12% vs 18%) and CD4⁺CD25⁺ (9.2% vs 16.9%) T-cell migration was significantly impaired on exposure to *Bdmc*^{-/-}-derived conditioned medium, supporting the hypothesis that *Ambra1*-deficient melanoma cells directly affect Treg migration to the TIME.

The signal mediated by the chemokine *Ccl22* and interleukin *Il-1 α* , triggered by cancer cell production/secretion of *Il-1 α* , has been previously demonstrated to promote Treg recruitment to the tumor.²⁷ Interestingly, loss of *Ambra1* led to a downregulation of *Il-1 α* (figures 1A,E and 4B,I) and *Ccl22* (figure 1E) at both transcriptional and secretional levels. Therefore, to investigate whether the *Ccl22*/*Il-1 α* signal could directly affect Treg infiltration on *Ambra1* deficiency, T-cell migration was assessed by supplementing *Il-1 α* to the conditioned media of *Bdmc*^{-/-} cells. A rescue in Treg cells migration capacity (12.8% vs 9.2%) (figure 4D), as well as an increase in splenocyte *Ccl22* expression (figure 4E), were observed in such settings, suggesting that *Il-1 α* -mediated signaling contributes to the reduced CD4⁺CD25⁺ Treg infiltration in *Ambra1*-deficient tumors.

Based on our recent findings regarding *Ambra1*'s negative regulation of FAK1 activity,¹⁰ we investigated a possible link between this molecular interplay and

decreased Treg migration upon *Ambra1* deficiency. As the nuclear fraction of FAK1 is known to regulate such events in the tumor microenvironment of squamous cell carcinoma,²⁸ NEs from *AMBRA1*-silenced SK-Mel-5 (figure 4F) and MeWo (online supplemental figure 5B,C) cells were analyzed. These data showed that the nuclear fraction of FAK1 remained unchanged independent of *AMBRA1* status (figure 4G and H and online supplemental figure 5B,D). To further investigate this aspect, SK-Mel-5 cells were transfected with a plasmid encoding a single-point mutant of *AMBRA1* (*AMBRA1*^{L110F}) (figure 4I), which resembles the *AMBRA1*-deficient phenotype (FAK1 oncogenic pathway and epithelial-mesenchymal transition (EMT) process activation, cyclin D1 stabilization).¹⁹ Only limited changes in the cytokine profile were observed in the conditioned media of *AMBRA1*^{L110F}-expressing cells (online supplemental figure 5E,F), together with no significant variations in interleukin (IL)-1 α secretion, if compared with *AMBRA1*^{WT}-expressing cells (figure 4K). However, RT-qPCR analyses revealed that, beyond rescued expression in *AMBRA1*^{WT}-expressing versus *AMBRA1*-silenced cells (figure 4L), a further significant increase in *Il-1 α* expression was detected in *AMBRA1*^{L110F}-expressing versus *AMBRA1*^{WT}-expressing cells (figure 4L). Interestingly, the *AMBRA1*^{L110F} mutant still retains the pro-autophagic role of *AMBRA1*,¹⁹ as no differences in the LC3 ratio were depicted in comparison with *AMBRA1*^{WT}-expressing cells (figure 4I and J). Therefore, to investigate whether the autophagy function of *AMBRA1* could be implicated instead, *Bdmc*^{+/+} cells were treated with the autophagy inhibitor CQ (online supplemental figure 5G,H). Similarly to *Ambra1* depletion (figure 4A and B), *Il-1 α* secretion decreased also on autophagy blockage in primary murine melanoma cells (online supplemental figure 5I,J).

Overall, these results suggest that the pro-autophagic function of *Ambra1*, rather than the previously identified tumorigenic functions of the protein,¹⁰ contributes to the cytokine changes induced by melanoma cells.

Ambra1 deficiency increases anti-PD-1 therapy response in *Braf*/*Pten*/*Cdkn2A*-driven melanoma

As the selective depletion of Treg has become a promising strategy to enhance the response to ICB therapy,²⁹⁻³¹ we sought to investigate whether reduced Treg infiltrating cells in *Ambra1*-deficient tumors could affect the response to PD-1 blockade. We first analyzed the correlation between *AMBRA1* expression and ICB treatment response in a publicly available data set of patients with advanced melanoma treated with anti-PD-1 therapy.²⁵ Despite the modest number of patients exhibiting CR, we discovered a positive, although not statistically significant, association between CR and low *AMBRA1* expression (figure 5A). To investigate if *Ambra1* could play a role in the response to anti-PD-1 therapy, YUMMI.7 cells³² were depleted for *Ambra1* by shRNAs and employed in a preclinical mouse

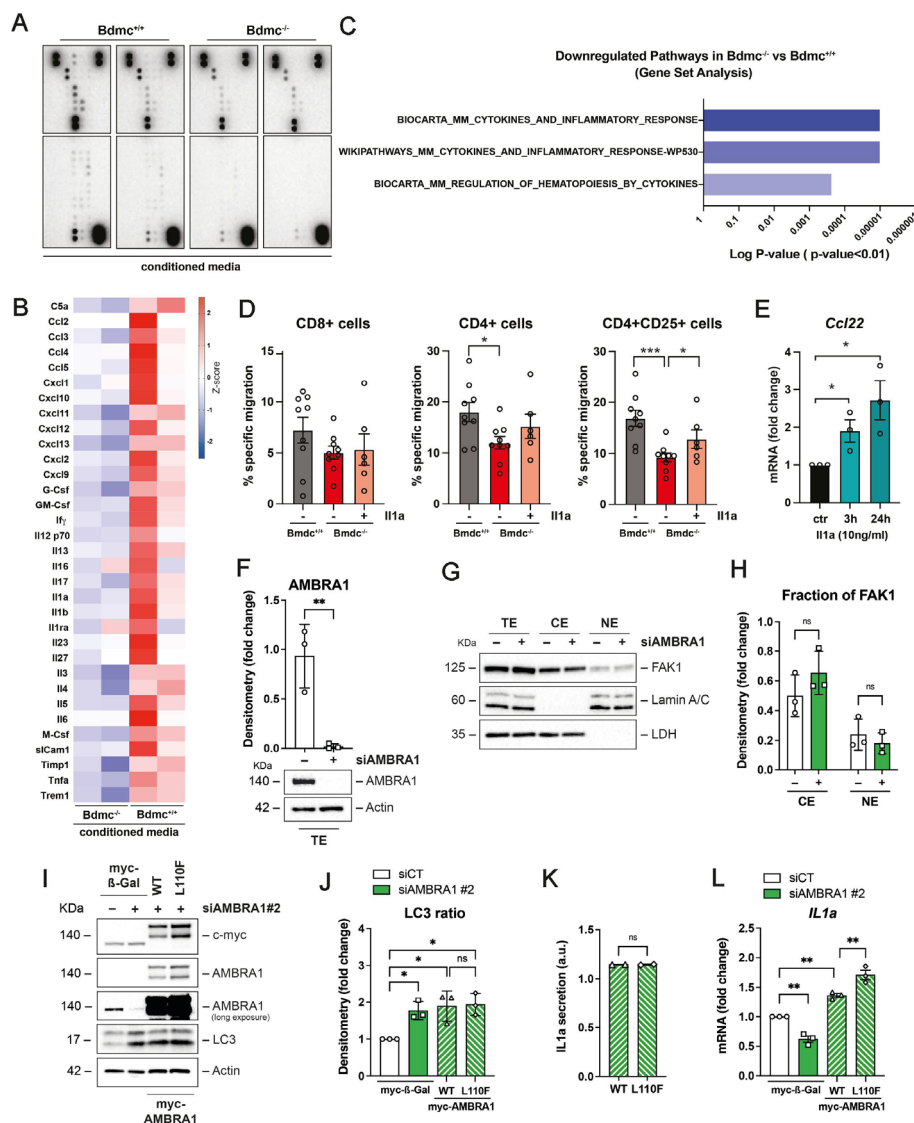


Figure 4 Analysis of T cells migration upon Ambra1 deficiency. (A) Representative images of the Mouse Cytokine Array in supernatants (conditioned media) of *Bdmc*^{+/+} (left) and *Bdmc*^{-/-} (right) cells. (B) The average pixel density (pair of duplicate spots represents each cytokine) was quantified and reported as fold change compared with *Bdmc*^{+/+}. The heat map of the less secreted cytokines by *Bdmc*^{-/-} cells compared with *Bdmc*^{+/+} is shown. (C) Gene set analysis (GSA) shows the downregulated pathways in Ambra1 deficiency conditions ($p < 0.01$) based on the differentially expressed cytokines in (B). Out of 33 cytokines included in the panel, 28 were found in the pathway database. For GSA, hypergeometric tests were used and genes with a p value < 0.01 and $\text{abs}(\log \text{FC}) > 1$ were considered as significant (*BioCarta* and *WikiPathways*). (D) Splenocytes were cultured in *Bdmc*^{+/+}, *Bdmc*^{-/-} or *Bdmc*^{-/-}/*Il-1 α* - (10 ng/mL) derived conditioned media for 26–28 hours and migration of CD3⁺CD8⁺, CD3⁺CD4⁺ and CD3⁺CD4⁺CD25⁺ T cells examined by flow cytometry. Error bars indicate SEM (* $p < 0.05$, *** $p < 0.001$, $n = 6–9$). (E) RT-qPCR analysis of *Ccl22* in splenocytes ($n = 3$) after *Il-1 α* administration at indicated times. Data were normalized to the internal control *L34* and expressed as fold change \pm SEM with respect to the untreated splenocytes (ctr) (* $p < 0.05$, 3 hours or 24 hours vs ctr). (F) AMBRA1 was silenced in SK-Mel-5 (siAMBRA1) for 48 hours and WB analyses ($n = 3$) performed to evaluate silencing (TE, total extracts). Actin was used as loading control. Data in the graph represent densitometry analyses and are shown as fold change \pm SD versus siCT cells (** $p < 0.01$). (G) Representative WB analyses ($n = 3$) of total (TE), cytosolic (CE) and nuclear (NE) extracts of SK-Mel-5 silenced for AMBRA1 as shown in (F). FAK1 was detected together with the purity controls lamin A/C (for TE) and LDH (for CE). (H) The cytosolic and nuclear fractions of FAK1 shown in (G) were quantified. Data are expressed as average \pm SD (ns, not significant). (I) Representative WB analyses ($n = 3$) of SK-Mel-5 re-expressing myc-tagged AMBRA1 mutants (WT and L110F). AMBRA1 and c-myc were detected to determine transfection efficiency; LC3 as marker of the autophagy flux; actin as loading control. (J) The autophagy marker LC3 shown in (I) was quantified. Data are expressed as fold change \pm SD ($n = 3$; * $p < 0.05$). (K) Secretion of *IL-1 α* was measured in supernatants of cells transfected as in (I). Each dot represents the average pixel density of a single membrane's duplet. Data are expressed as arbitrary unit \pm SD ($n = 2$; ns, not significant). (L) RT-qPCR analysis of *IL-1 α* in SK-Mel-5 transfected as in (I). Data were normalized to the internal control *RPLP0* and expressed as fold change \pm SEM (** $p < 0.01$). Ambra1, focal adhesion kinase 1; IL, interleukin; LDH, lactate dehydrogenase; RT-qPCR, real-time quantitative PCR; WB, western blot.

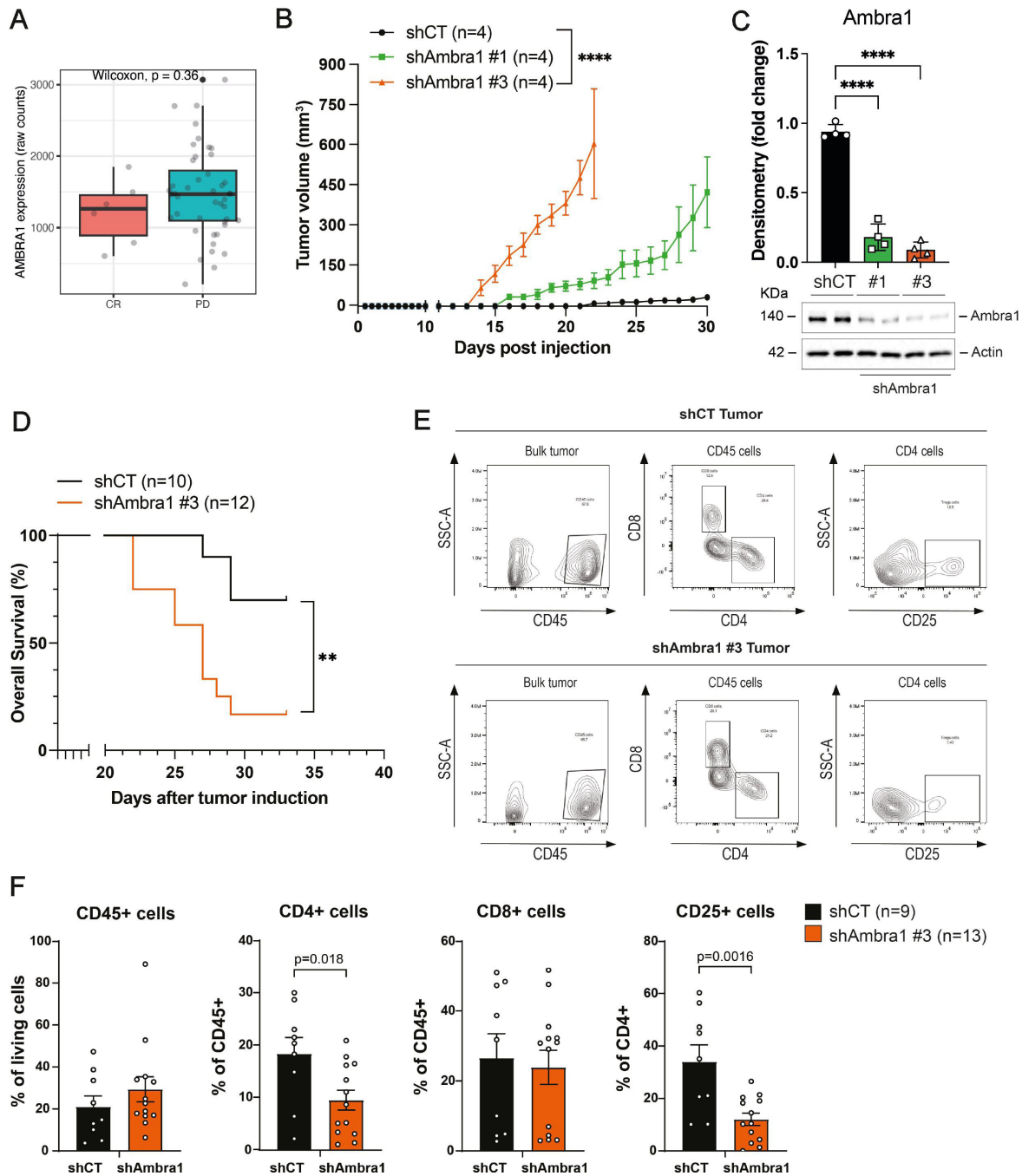


Figure 5 AMBRA1 expression in patients with anti-PD-1 treated melanoma and effects of Ambra1 deletion in syngeneic mice. (A) Raw counts were downloaded from the Gene Expression Omnibus (GSE91061). Patient-derived data, directly downloaded from the author's publication, were filtered with extreme response profiles to anti-PD-1 treatment (nivolumab; CR, complete response; PD, progressive disease) and AMBRA1 expression was compared between both groups. Pretreatment and on-treatment samples were both kept. (B) Volume of tumors of syngeneic mice injected with shCT (n=4), shAmbra1 #1 (n=4) and #3 (n=4) YUMM1.7 cells. Each data point corresponds to the average tumor volume \pm SEM, as determined for each experimental group (**** $p < 0.0001$). (C) Ambra1 expression was determined in tumors from syngeneic mice injected with shCT (n=4), shAmbra1 #1 (n=4) and shAmbra1 #3 (n=4) YUMM1.7 cells by WB. Actin was used as loading control. Data in the graph represent densitometry analyses and are shown as fold change \pm SD versus shCT cells (n=4; **** $p < 0.0001$). (D) Overall survival of syngeneic mice injected with shCT (n=10) and shAmbra1 #3 (n=12) YUMM1.7 cells. Log-rank test for comparisons of Kaplan-Meier survival curves indicates lower survival in shAmbra1 #3 versus shCT (** $p < 0.01$). (E–F) Tumors from shCT (n=9) and shAmbra1 #3 (n=13) syngeneic mice were collected and processed for flow cytometric analysis. Quantification is reported as a percentage of indicated cell type among live cells or the parental gate. (E) Representative flow plots on the gating strategy of shCT and shAmbra1 #3 tumors. (F) % of CD45⁺ cells out of the live cell population; % of CD4⁺ (defined as CD45⁺CD4⁺), CD8⁺ (defined as CD45⁺CD8⁺) and CD25⁺ (defined as CD45⁺CD4⁺CD25⁺) cells out of the parental gate. Each dot represents one mouse and corresponds to mean \pm SEM. Data were analyzed by unpaired t-test (shAmbra1 #3 vs shCT). Ambra1, autophagy and beclin 1 regulator 1; GSE, gene set enrichment; PD-1, programmed cell death protein 1; WB, western blot.

model of melanoma, which was reported to exhibit a limited tumor inhibition following treatment with PD-1 inhibitors.^{33–35} We first confirmed the Ambra1-related functions in autophagy, cell proliferation and invasion¹⁰ in shAmbra1 (#1 and #3; shRNAs targeting different regions of Ambra1) versus shCT (control shRNA) YUMMI.7 cells (online supplemental figure 6A,B). Then, shAmbra1 #1 and #3, as well as shCT YUMMI.7 cells, were subcutaneously injected in C57BL/6 immunocompetent mice. As shown in figure 5B and C, Ambra1 knock-down tumors (shAmbra1 #1 and shAmbra1 #3) displayed accelerated tumor growth, particularly shAmbra1 #3 tumors. Therefore, the shAmbra1 #3-derived model was chosen for the following analyses and validated in terms of tumor growth kinetics (online supplemental figure 6C) and overall survival (figure 5D). We also investigated T-cell infiltrates in shAmbra1 #3 melanomas compared with their shCT counterparts. Flow cytometry analysis in figure 5E and F showed that CD4⁺ (9.5% vs 18.4%) and CD4⁺CD25⁺ (12% vs 34%) cells were significantly reduced in Ambra1-knockdown tumors relative to the control, and none of these differences was found in matched spleens (online supplemental figure 6D,E).

We then treated shAmbra1 #3 and shCT syngeneic mice with an anti-PD-1 antibody (aPD-1) and an isotype control (IgG) for at least 15 days after the tumor was palpable. Despite complete tumor regression was not observed, our results revealed that the aPD-1 regimen was more effective in reducing kinetics of tumor growth in Ambra1-knockdown tumors (shAmbra1 #3 aPD-1), at least within 15 days of treatment, compared with control (IgG-treated) counterparts (figure 6A). As expected, shCT-derived tumors did not respond to PD-1 inhibition (shCT aPD-1) and displayed kinetics similar to the IgG-treated shCT tumors (figure 6A). The overall survival analysis also showed that, while IgG-treated shAmbra1 #3 tumors reached earlier the maximally tolerated size, aPD-1-treated shAmbra1 #3 did it in a time frame comparable to shCT tumors (figure 6B).

Overall, these results indicated that the absence of Ambra1, while promoting melanoma growth in a *Braf*^{V600E/+}; *Pten*^{-/-}; *Cdkn2A*^{-/-} genetic background, enhanced the response to PD-1 blockade.

DISCUSSION

Metastatic melanoma is among the most responsive cancers to immune checkpoint inhibitors due to its high tumor mutational burden and immunogenicity.⁴ Yet, only a subgroup of patients gain significant clinical benefit from this treatment.^{3 4 36} An important factor in determining tumor immunogenicity and response to ICB therapy is the composition of the TIME, including the balance between activated T cells and immune-suppressive cells infiltrating the tumor.⁷ In this study, we demonstrated that deletion of the melanoma suppressor *Ambra1* (1) was associated with reduced cytokine-mediated inflammatory signaling and (2) strongly inhibited tumor infiltration

of immunosuppressive Treg in transgenic and syngeneic models of melanoma. These findings were corroborated in human melanoma samples, showing a correlation between low *AMBRA1* expression and a low number of Treg. Interestingly, the selective inhibition of immunosuppressive Treg has been explored for several years as an alternative strategy to enhance the ability of ICB therapy to kill the tumor.^{29–31 37–39} Recently, a specific Fc-optimized anti-CD25 antibody (*RG6292*) has been developed to selectively target Treg cells into the tumor without leading to immune-related toxicities and preserving the IL-2 signaling on effector T cells.^{37 39} Interestingly, this antibody was demonstrated to synergize with ICB therapy to eradicate tumors³⁷ and is currently undergoing a clinical trial to evaluate its safety and tolerability in patients with advanced solid tumors (NCT04158583).

In our study, Ambra1-deficient tumors exhibited a partial reduction of tumor growth on anti-PD-1 treatment, suggesting that Ambra1 status might affect responsiveness to ICB therapy. By analyzing transcriptomic data from advanced melanomas, low *AMBRA1* levels and response to anti-PD-1 treatment seem to show a trend association, likely due to limitations in terms of number of responders and data on *AMBRA1* expression restricted to RNA levels. A complete tumor regression was not detected in anti-PD-1-treated Ambra1-deficient mice in the time frame of our in vivo study. Most likely, such incomplete response can be ascribed to the proliferative advantage of null or low-expressing Ambra1 tumor cells,¹⁰ as also shown by accumulation of cyclin D1 in shAmbra1 (#1 and #3) YUMMI.7 cells. This is indeed a typical feature observed upon Ambra1 loss, which may overcome the immune response activated by the PD-1 inhibitor, eventually leading to maintained tumor growth.

The immune-modulatory effects of Ambra1 are explained at least in part by changes in the expression and secretion of specific ILs and chemokines directly affecting Treg infiltration. Intriguingly, it has been revealed that Ccl22-IL-1 α -mediated signaling, induced by cancer cell release of IL-1 α , promotes Treg recruitment to the tumor.²⁷ In our setting, loss of Ambra1 led to down-regulation of IL-1 α and the Treg-attracting chemokine Ccl22, and suppression of Treg infiltration in Ambra1-null tumors was rescued by supplementing IL-1 α . Together, these findings point to the Ambra1-IL-1 α -Ccl22 signaling axis as a possible mechanism underlying the reduction of Treg infiltration in Ambra1-deficient melanoma.

Ambra1 has been described as a positive regulator of autophagy, interacting with several proteins involved in the different steps of the autophagy process.^{14–17} Autophagy has been reported to specifically modulate the production and secretion of IL-1 family cytokines (eg, IL-18, IL-1 α and β) as well as chemokines (eg, Ccl5) via different mechanisms.^{40–45} Although we previously showed that the tumor-suppressive role of Ambra1 in melanoma was beyond its autophagy function,^{10 46} the results obtained with the expression of a mutant form of *AMBRA1* point to a role for *AMBRA1*-mediated

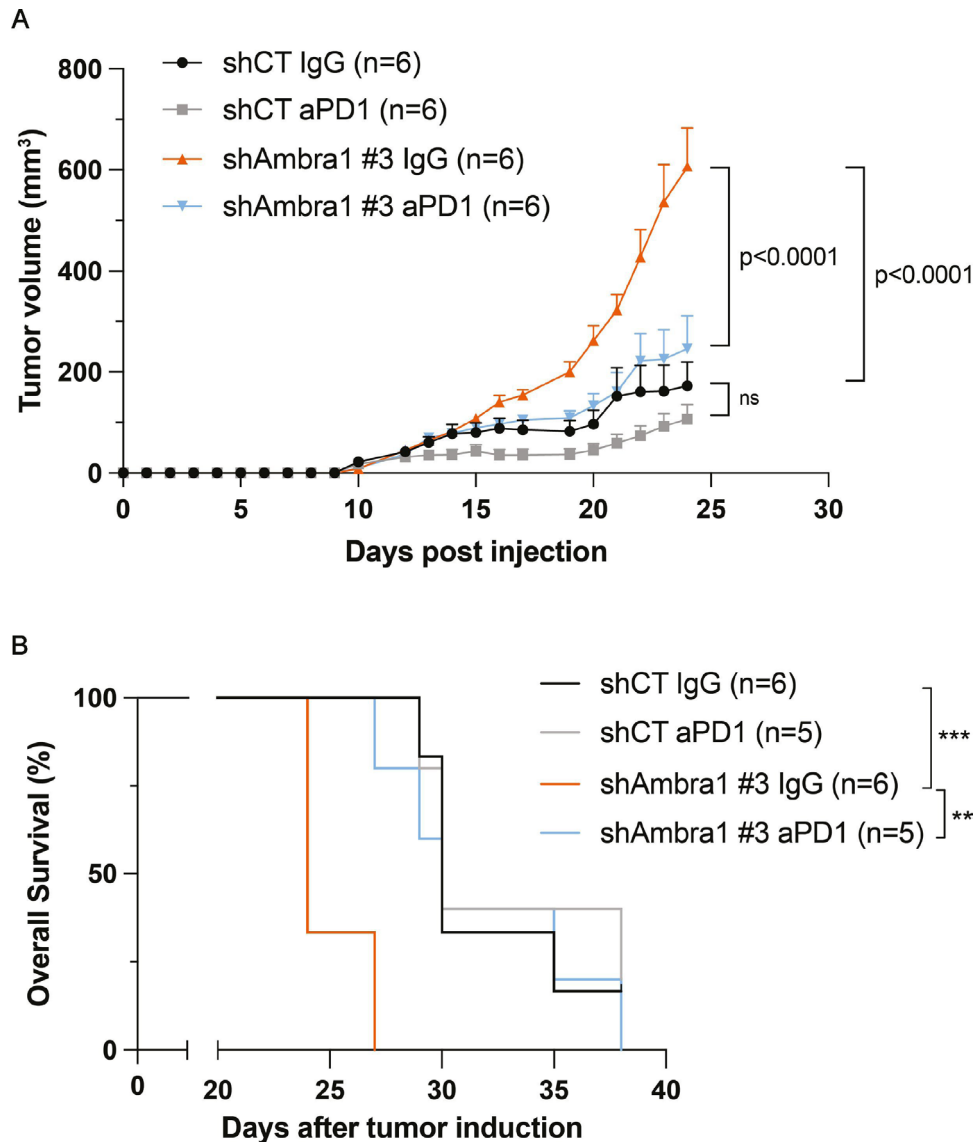


Figure 6 Analysis of PD-1 inhibitor treatment in Ambra1-deficient tumors. (A) Tumor kinetics in mice receiving 150,000 shCT or shAmbra1 #3 YUMM1.7 cells. When tumors were measurable, mice were assigned to receive anti-PD-1 (aPD-1) or isotype control (IgG) injections and the tumor kinetics was evaluated for 15 days (n=6). Each data point corresponds to the average tumor volume \pm SEM, as determined for each experimental group. (B) Overall survival of syngeneic mice injected with shCT (n=5–6) and shAmbra1 #3 (n=5–6) YUMM1.7 cells, treated with aPD-1/IgG. The endpoint was defined as the date the mice reached tumor max size. Log-rank test for comparisons of Kaplan-Meier survival curves indicates lower survival in shAmbra1 #3 IgG versus shAmbra1 #3 aPD-1 (**p<0.01), and in shAmbra1 #3 IgG versus shCT aPD-1/IgG (**p<0.001). Ambra1, autophagy and beclin 1 regulator 1; aPD-1, anti-PD-1 antibody; PD-1, programmed cell death protein 1.

autophagy in regulating cytokine signaling, specifically IL-1 α , and possibly Treg infiltration. Indeed, this mutant retains the autophagic function of the protein, while resembling the AMBRA1-deficient phenotype in melanoma (eg, FAK1 activation, cyclin D1 accumulation and EMT induction¹⁹). However, which are the exact mechanisms by which autophagy can modulate IL-1 α expression in cancer cells, or whether the sole autophagy function of AMBRA1 (rather than additional unknown functions) is the only mechanism involved in this regulation, deserve further investigation.

Our study adds *Ambra1* to the growing list of cancer genes that, in addition to their canonical tumor

suppressor functions, contribute to modulate the TIME through tumor cell-intrinsic expression of cytokines and chemokines. In melanoma, constitutive activation of MAPK signaling mediated by the BRAF^{V600E} oncogene leads to increased production of the pro-inflammatory cytokines such as IL-6 and IL-10, contributing to melanoma cell evasion of the immune system.⁴⁷ Similarly, oncogenic *KRAS* mutations have been shown to induce a pro-inflammatory and immunosuppressive stroma in multiple cancer types.⁴⁸ Ambra1 is an intrinsically disordered protein that can interact with several protein partners.^{11 49} This multifaceted nature has undoubtedly conferred Ambra1 numerous functions, ranging from

autophagy to apoptosis, cell proliferation and invasion, which may differently, either in synergy or not, affect tumor progression and response to therapy.^{11 49} Hence, *Ambra1* may represent a new class of cancer genes the absence or downregulation of which, in contrast to oncogenic *BRAF* and *KRAS*, suppresses inflammation and increases the response to immunotherapy alongside promoting tumorigenesis.

In conclusion, our work sheds light on *Ambra1* as a modulator of the TIME in melanoma. Whether patients stratified for null/low *AMBRA1* expression could display a better response to ICB therapy as a consequence of a lower number of Treg cells, hence highlighting these cells as a promising therapeutic target for immunotherapy efficacy, awaits further studies.

Author affiliations

¹Melanoma Research Team, Center for Autophagy, Recycling and Disease (CARD), Danish Cancer Society Research Center, Copenhagen, Denmark

²Lab of Translational Cell and Tissue Research, KU Leuven, Leuven, Belgium

³National Center for Cancer Immunotherapy, Department of Oncology, Copenhagen University Hospital, Herlev, Denmark

⁴Molecular Diagnostics Group, Danish Cancer Society Research Center, Copenhagen, Denmark

⁵INSERM U981 and Department of Oncologic Medicine, Gustave Roussy Institute and Paris Saclay University, Villejuif, France

⁶Department of Life Sciences and Medicine, University of Luxembourg, Belvaux, Luxembourg

⁷Department of Cancer and Inflammation Research, Institute for Molecular Medicine, University of Southern Denmark, Odense, Denmark

⁸Cell Stress and Survival, Center for Autophagy, Recycling and Disease (CARD), Danish Cancer Society Research Center, Copenhagen, Denmark

⁹Fondazione Policlinico Universitario Agostino Gemelli IRCCS, Rome, Italy

¹⁰Department of Drug Design and Pharmacology, Faculty of Health and Medical Sciences, University of Copenhagen, Copenhagen, Denmark

Twitter Daniela De Zio @melanomateam

Contributors Conception and design: AF, DDZ. Development of methodology: AF, LN, AA, LDL, MC, VB, GC, DDZ. Acquisition of data: AF, LDL, CP, CD, LN, MC, GEM, MDA. Analysis and interpretation of data: AF, LDL, CP, CD, AA, MC, VB, GEM, MDA, MPP, TS, FMB, DDZ. Writing, review and/or revision of the manuscript: DDZ, PG, LDL (all authors have reviewed and edited the manuscript). Administrative, technical, or material support: CR, DHM, FC, DDZ. Guarantor: DDZ. Study supervision: DDZ.

Funding The authors acknowledge the staff of the Animal Facility at the Danish Cancer Society and Laila Fischer for help with secretarial work. This project has received financial support from the Danish Cancer Society (R204-A12424 to DDZ and R231-A14035 to DHM), the LEO Foundation (LF-OC-19-000004 to DDZ, LF17024 to FC) and Lundbeck Foundation (R307-2018-3326 to DHM). DDZ is supported by the NEYE foundation and the Melanoma Research Alliance young investigator grant (MRA 620385). The Melanoma Research Team is part of the Center of Excellence for Autophagy, Recycling and Disease (CARD), funded by Danmarks Grundforskningsfond (DNRF125).

Competing interests None declared.

Patient consent for publication Not applicable.

Provenance and peer review Not commissioned; externally peer reviewed.

Data availability statement Data are available in a public, open access repository. All data relevant to the study are included in the article or uploaded as supplementary information. The RNAseq data analyzed during the current study are public available under the GEO accession number GSE151134 and GSE91061. The NanoString data generated and analyzed during the current study are available in online supplemental tables 1 and 2.

Supplemental material This content has been supplied by the author(s). It has not been vetted by BMJ Publishing Group Limited (BMJ) and may not have been peer-reviewed. Any opinions or recommendations discussed are solely those

of the author(s) and are not endorsed by BMJ. BMJ disclaims all liability and responsibility arising from any reliance placed on the content. Where the content includes any translated material, BMJ does not warrant the accuracy and reliability of the translations (including but not limited to local regulations, clinical guidelines, terminology, drug names and drug dosages), and is not responsible for any error and/or omissions arising from translation and adaptation or otherwise.

Open access This is an open access article distributed in accordance with the Creative Commons Attribution Non Commercial (CC BY-NC 4.0) license, which permits others to distribute, remix, adapt, build upon this work non-commercially, and license their derivative works on different terms, provided the original work is properly cited, appropriate credit is given, any changes made indicated, and the use is non-commercial. See <http://creativecommons.org/licenses/by-nc/4.0/>.

ORCID iDs

Luca Di Leo <http://orcid.org/0000-0002-2419-2196>

Loulieta Nazerai <http://orcid.org/0000-0002-1090-9029>

Chiara Pagliuca <http://orcid.org/0000-0002-1694-0342>

Daniela De Zio <http://orcid.org/0000-0002-9454-402X>

REFERENCES

- Shain AH, Bastian BC. From melanocytes to melanomas. *Nat Rev Cancer* 2016;16:345–58.
- Shain AH, Joseph NM, Yu R, et al. Genomic and transcriptomic analysis reveals incremental disruption of key signaling pathways during melanoma evolution. *Cancer Cell* 2018;34:45–55.
- Luke JJ, Flaherty KT, Ribas A, et al. Targeted agents and immunotherapies: optimizing outcomes in melanoma. *Nat Rev Clin Oncol* 2017;14:463–82.
- Huang AC, Zappasodi R. A decade of checkpoint blockade immunotherapy in melanoma: understanding the molecular basis for immune sensitivity and resistance. *Nat Immunol* 2022;23:660–70.
- Robert C. A decade of immune-checkpoint inhibitors in cancer therapy. *Nat Commun* 2020;11:3801.
- Carlini MS, Larkin J, Long GV. Immune checkpoint inhibitors in melanoma. *Lancet* 2021;398:1002–14.
- Morad G, Helmink BA, Sharma P, et al. Hallmarks of response, resistance, and toxicity to immune checkpoint blockade. *Cell* 2021;184:5309–37.
- Barnes TA, Amir E. Hype or hope: the prognostic value of infiltrating immune cells in cancer. *Br J Cancer* 2017;117:451–60.
- Binnewies M, Roberts EW, Kersten K, et al. Understanding the tumor immune microenvironment (time) for effective therapy. *Nat Med* 2018;24:541–50.
- Di Leo L, Bodemeyer V, Bosisio FM, et al. Loss of *ambra1* promotes melanoma growth and invasion. *Nat Commun* 2021;12:2550.
- Cianfanelli V, De Zio D, Di Bartolomeo S, et al. *Ambra1* at a glance. *J Cell Sci* 2015;128:2003–8.
- Cianfanelli V, Fuoco C, Lorente M, et al. *AMBRA1* links autophagy to cell proliferation and tumorigenesis by promoting c-myc dephosphorylation and degradation. *Nat Cell Biol* 2015;17:20–30.
- Maiani E, Milletti G, Nazio F, et al. *AMBRA1* regulates cyclin D to guard S-phase entry and genomic integrity. *Nature* 2021;592:799–803.
- Fimia GM, Stoykova A, Romagnoli A, et al. *Ambra1* regulates autophagy and development of the nervous system. *Nature* 2007;447:1121–5.
- Di Bartolomeo S, Corazzari M, Nazio F, et al. The dynamic interaction of *AMBRA1* with the dynein motor complex regulates mammalian autophagy. *J Cell Biol* 2010;191:155–68.
- Strappazzon F, Di Rita A, Cianfanelli V, et al. Prosurvival *AMBRA1* turns into a proapoptotic BH3-like protein during mitochondrial apoptosis. *Autophagy* 2016;12:963–75.
- Strappazzon F, Nazio F, Corrado M, et al. *AMBRA1* is able to induce mitophagy via LC3 binding, regardless of parkin and p62/SQSTM1. *Cell Death Differ* 2015;22:419–32.
- Bolognesi MM, Manzoni M, Scalia CR, et al. Multiplex staining by sequential immunostaining and antibody removal on routine tissue sections. *J Histochem Cytochem* 2017;65:431–44.
- Tiberti M, Di Leo L, Vistesen MV, et al. The cancerMuts software package for the prioritization of missense cancer variants: a case study of *AMBRA1* in melanoma. *Cell Death Dis* 2022;13:872.
- Di Leo L, Vegliante R, Ciccarone F, et al. Forcing ATGL expression in hepatocarcinoma cells imposes glycolytic rewiring through PPAR- α /p300-mediated acetylation of p53. *Oncogene* 2019;38:1860–75.
- Vandesompele J, De Preter K, Pattyn F, et al. Accurate normalization of real-time quantitative RT-PCR data by geometric

- averaging of multiple internal control genes. *Genome Biol* 2002;3:RESEARCH0034.
- 22 Våremo L, Nielsen J, Nookaew I. Enriching the gene set analysis of genome-wide data by incorporating directionality of gene expression and combining statistical hypotheses and methods. *Nucleic Acids Res* 2013;41:4378–91.
 - 23 Chen B, Khodadoust MS, Liu CL, et al. Profiling tumor infiltrating immune cells with CIBERSORT. *Methods Mol Biol* 2018;1711:243–59.
 - 24 Hu H, Miao YR, Jia LH, et al. AnimalTFDB 3.0: a comprehensive resource for annotation and prediction of animal transcription factors. *Nucleic Acids Res* 2019;47:D33–8.
 - 25 Riaz N, Havel JJ, Makarov V, et al. Tumor and microenvironment evolution during immunotherapy with nivolumab. *Cell* 2017;171:934–49.
 - 26 Antoranz A, Van Herck Y, Bolognesi MM, et al. Mapping the immune landscape in metastatic melanoma reveals localized cell-cell interactions that predict immunotherapy response. *Cancer Res* 2022;82:3275–90.
 - 27 Wiedemann GM, Knott MML, Vetter VK, et al. Cancer cell-derived IL-1 α induces CCL22 and the recruitment of regulatory T cells. *Oncoimmunology* 2016;5:e1175794.
 - 28 Serrels A, Lund T, Serrels B, et al. Nuclear FAK controls chemokine transcription, tregs, and evasion of anti-tumor immunity. *Cell* 2015;163:160–73.
 - 29 Ouyang Z, Wu H, Li L, et al. Regulatory T cells in the immunotherapy of melanoma. *Tumour Biol* 2016;37:77–85.
 - 30 Jacobs JFM, Nierkens S, Figdor CG, et al. Regulatory T cells in melanoma: the final hurdle towards effective immunotherapy? *Lancet Oncol* 2012;13:e32–42.
 - 31 Huang L, Guo Y, Liu S, et al. Targeting regulatory T cells for immunotherapy in melanoma. *Mol Biomed* 2021;2:11.
 - 32 Meeth K, Wang JX, Micevic G, et al. The YUMM lines: a series of congenic mouse melanoma cell lines with defined genetic alterations. *Pigment Cell Melanoma Res* 2016;29:590–7.
 - 33 Homet Moreno B, Zaretsky JM, Garcia-Diaz A, et al. Response to programmed cell death-1 blockade in a murine melanoma syngeneic model requires costimulation, CD4, and CD8 T cells. *Cancer Immunol Res* 2016;4:845–57.
 - 34 Lelliott EJ, Cullinane C, Martin CA, et al. A novel immunogenic mouse model of melanoma for the preclinical assessment of combination targeted and immune-based therapy. *Sci Rep* 2019;9:1225.
 - 35 Wang J, Perry CJ, Meeth K, et al. Uv-Induced somatic mutations elicit a functional T cell response in the YUMMER1.7 mouse melanoma model. *Pigment Cell Melanoma Res* 2017;30:428–35.
 - 36 Sharma P, Hu-Lieskovan S, Wargo JA, et al. Primary, adaptive, and acquired resistance to cancer immunotherapy. *Cell* 2017;168:707–23.
 - 37 Arce Vargas F, Furness AJS, Solomon I, et al. Fc-optimized anti-CD25 depletes tumor-infiltrating regulatory T cells and synergizes with PD-1 blockade to eradicate established tumors. *Immunity* 2017;46:577–86.
 - 38 Arce Vargas F, Furness AJS, Litchfield K, et al. Fc effector function contributes to the activity of human anti-CTLA-4 antibodies. *Cancer Cell* 2018;33:649–63.
 - 39 Solomon I, Amann M, Goubier A, et al. CD25-Treg-depleting antibodies preserving IL-2 signaling on effector T cells enhance effector activation and antitumor immunity. *Nat Cancer* 2020;1:1153–66.
 - 40 Harris J. Autophagy and IL-1 family cytokines. *Front Immunol* 2013;4:83.
 - 41 Mgrditchian T, Arakelian T, Paggetti J, et al. Targeting autophagy inhibits melanoma growth by enhancing NK cells infiltration in a CCL5-dependent manner. *Proc Natl Acad Sci U S A* 2017;114:E9271–9.
 - 42 Monkkonen T, Debnath J. Inflammatory signaling cascades and autophagy in cancer. *Autophagy* 2018;14:190–8.
 - 43 Crişan TO, Plantinga TS, van de Veerdonk FL, et al. Inflammasome-independent modulation of cytokine response by autophagy in human cells. *PLoS One* 2011;6:e18666.
 - 44 Criollo A, Chereau F, Malik SA, et al. Autophagy is required for the activation of NF κ B. *Cell Cycle* 2012;11:194–9.
 - 45 Giegerich AK, Kuchler L, Sha LK, et al. Autophagy-Dependent PELI3 degradation inhibits proinflammatory IL1B expression. *Autophagy* 2014;10:1937–52.
 - 46 Di Leo L, De Zio D. AMBRA1 has an impact on melanoma development beyond autophagy. *Autophagy* 2021;17:1802–3.
 - 47 Sumimoto H, Imabayashi F, Iwata T, et al. The BRAF-MAPK signaling pathway is essential for cancer-immune evasion in human melanoma cells. *J Exp Med* 2006;203:1651–6.
 - 48 Hamarshah S, Groß O, Brummer T, et al. Immune modulatory effects of oncogenic KRAS in cancer. *Nat Commun* 2020;11:5439.
 - 49 Li X, Lyu Y, Li J, et al. AMBRA1 and its role as a target for anticancer therapy. *Front Oncol* 2022;12:946086.